Remote Super-Resolution Mapping of Wave Fields

Jian-yu Lu[1]

[1]Affiliation not available

February 10, 2025

Abstract

Mapping wave field in space has many applications such as optimizing design of radio antennas, improving and developing ultrasound transducers, and planning and monitoring the treatment of tumors using high-intensity focused ultrasound (HIFU). Currently, there are methods that can map wave fields remotely or locally. However, there are limitations with these methods. For example, when mapping the wave fields remotely, the spatial resolution is limited due to a poor diffraction-limited resolution of the receiver, especially when the f-number of the receiver is large. To map the wave fields locally, the receiver is either subject to damage in hazardous environments (corrosive media, high temperature, and high wave intensity, etc) or difficult to be placed inside an object. To address these limitations, in this paper, the PSF-modulation super-resolution imaging method (January, 2024 IEEE TUFFC) was applied to map pulse ultrasound wave fields remotely at a high spatial resolution, overcoming the diffraction limit of a focused receiver. For example, to map a pulse ultrasound field of a full-width-at-half-maximum (FWHM) beam width of 1.24 mm at the focal distance of a transmitter, the FWHM beam widths of the super-resolution mapping of the pulse wave field with a spherical glass modulator of 0.7-mm diameter at two receiver angles (0o and 45o) were about 1.13 mm and 1.22 mm respectively, which were close to the theoretical value of 1.24 mm and were much smaller than the diffraction-limited resolution (1.81 mm) of the receiver. Without using the super-resolution method to remotely map the same pulse wave field, the FWHM beam width was about 2.06 mm. For comparison, the FWHM beam width obtained with a broadband (1-20 MHz) and 0.6-mm diameter polyvinylidene fluoride (PVDF) needle hydrophone was about 1.41 mm. In addition to the focused pulse ultrasound wave field, a pulse Bessel beam near the transducer surface was mapped remotely with the super-resolution method, which revealed high spatial frequency components of the beam.

Remote Super-Resolution Mapping of Wave Fields

Jian-yu Lu, *Fellow*, *IEEE*

***Abstract*— Mapping wave field in space has many applications such as optimizing design of radio antennas, improving and developing ultrasound transducers, and planning and monitoring the treatment of tumors using high-intensity focused ultrasound (HIFU). Currently, there are methods that can map wave fields remotely or locally. However, there are limitations with these methods. For example, when mapping the wave fields remotely, the spatial resolution is limited due to a poor diffraction-limited resolution of the receiver, especially when the *f*-number of the receiver is large. To map the wave fields locally, the receiver is either subject to damage in hazardous environments (corrosive media, high temperature, and high wave intensity, etc) or difficult to be placed inside an object. To address these limitations, in this paper, the PSF-modulation super-resolution imaging method (January, 2024 IEEE TUFFC) was applied to map pulse ultrasound wave fields remotely at a high spatial resolution, overcoming the diffraction limit of a focused receiver. For example, to map a pulse ultrasound field of a full-width-at-half-maximum (FWHM) beam width of 1.24 mm at the focal distance of a transmitter, the FWHM beam widths of the super-resolution mapping of the pulse wave field with a spherical glass modulator of 0.7-mm diameter at two receiver angles (0^o and 45^o) were about 1.13 mm and 1.22 mm respectively, which were close to the theoretical value of 1.24 mm and were much smaller than the diffraction-limited resolution (1.81 mm) of the receiver. Without using the super-resolution method to remotely map the same pulse wave field, the FWHM beam width was about 2.06 mm. For comparison, the FWHM beam width obtained with a broadband (1-20 MHz) and 0.6-mm diameter polyvinylidene fluoride (PVDF) needle hydrophone was about 1.41 mm. In addition to the focused pulse ultrasound wave field, a pulse Bessel beam near the transducer surface was mapped remotely with the super-resolution method, which revealed high spatial frequency components of the beam.**

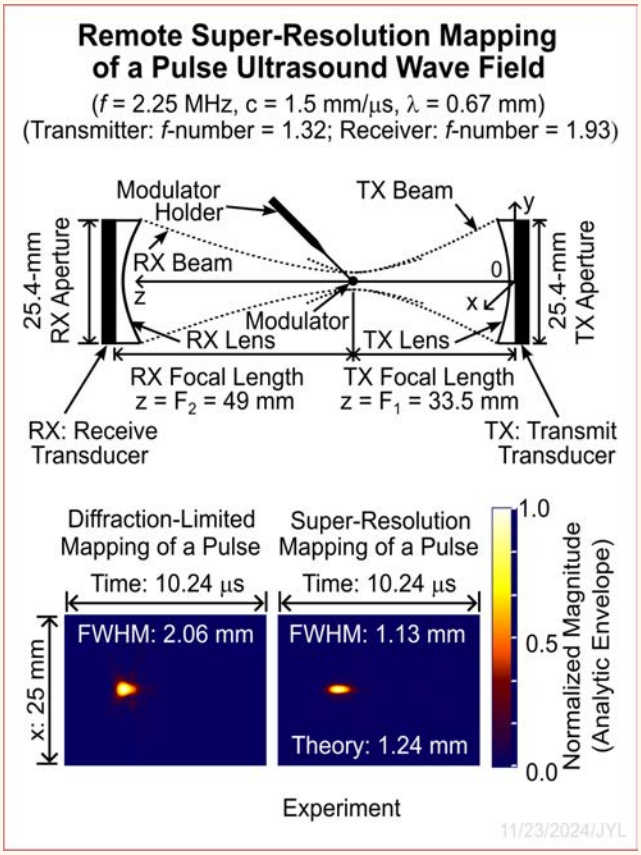

***Index Terms*— Electromagnetic, linear shift-invariant (LSI) system, linear time-invariant (LTI) system, modulation, modulator, optics, point spread function (PSF), super-resolution imaging, ultrasound, wave field mapping**

I. Introduction

Mapping of wave fields in space has many applications in both science and engineering. For example, mapping of electromagnetic waves can help in circuit design [1], antenna optimization [2], and understanding of the interactions between materials and the electromagnetic waves [3]. In ultrasound, there are also many applications in mapping of wave fields. These include mapping high-intensity focused ultrasound (HIFU) beam for targeted therapy, and planning and monitoring of tumor treatment [4]-[6]; mapping ultrasound transducer radiation patterns to improve transducer designs and characterizations [7]-[9], and optimize ultrasound beams for medical imaging [10] and nondestructive evaluation (NDE) of materials [11].

To map a wave field, a sensor of a small size can be placed in the field point by point in space. Small sensor size can reduce the spatial average effects of the sensor aperture and thus increase the spatial resolution of the mapped wave field [12]. However, small sensors are usually delicate, fragile, and

Jian-yu Lu is with the Department of Bioengineering, The University of Toledo, Toledo, Ohio 43606, USA. (e-mail: jian-yu.lu@ieee.org).

Highlights

- **A method for super-resolution mapping of wave fields remotely has been developed and a theoretical background was given, overcoming the diffraction limit.**
- **The experiments show that the method can be used for super-resolution mapping of pulse ultrasound wave fields remotely.**
- **This method has a potential to remotely mapping any wave fields both inside and outside an object, and thus may help in antenna design, transducer development and characterization, and ultrasound therapy.**

less sensitive. In the case of ultrasound, a small Polyvinylidene fluoride (PVDF) hydrophone is usually used to map ultrasound wave field [13]. Such a hydrophone can be damaged at high ultrasound intensity, high temperature, or in corrosive media. It also has a small capacitance and thus has high output impedance, which makes it difficult to drive a long cable. In addition, its sensitivity is usually lower than that of a larger focused transducer.

For mapping ultrasound wave fields of a higher intensity, lead zirconate titanate (PZT) transducers that are more robust than the PVDF hydrophones can be used [14]. However, such transducers also have a limitation in the power that they can handle before nonlinearity and thermal effects start to impact their performance. Alternatively, ultrasound wave fields of a range of intensities can be mapped by optical fibers that are based on Fresnel reflection from the tip surface of the fiber, two-beam interferometer to detect phase change between the measurement and reference beams, or Fabry–Perot interferometer that increases its sensitivity by multiple reflections within two parallel mirrors on the fiber tip, etc [15]. Some of the optical fiber methods can map the ultrasound wave fields at a very high intensity. However, optical fiber systems are much more expensive than those using either a PVDF hydrophone or a PZT transducer.

To avoid damaging delicate sensors such as PVDF hydrophones at a high ultrasound intensity or in a hazardous environment, a small scattering object such as the tip of an optical fiber has been used to scatter ultrasound waves that are then received by a larger transducer to map or characterize the ultrasound wave fields [15]-[23]. However, such method cannot be used when there are other scattering objects such as biological soft tissues in the wave fields to be mapped, or, when part of the ultrasound waves from the wave source can reach the receiver directly.

All of the methods above are difficult to measure ultrasound wave field inside objects such as biological soft tissues since it is difficult to place a PDVF hydrophone, a PZT transducer, or an optical fiber at various spatial points inside the objects. To overcome such difficulties, a large focused ultrasound transducer can be placed remotely outside the objects and then the focal point of the transducer can be scanned from one spatial position to another to map the ultrasound wave fields inside the objects. However, there are a few problems with this approach: Firstly, due to refraction, reflection, scattering, and attenuation of ultrasound waves inside some objects, it may be difficult to know the positions of the focal point of the receiver. Secondly, the scattering coefficient inside the objects may change from one spatial position to another, which can cause object-dependent errors when mapping the ultrasound wave fields inside the objects. Thirdly, the focused receiver has a diffraction limited resolution that is usually much larger than one-half of a wavelength of the ultrasound wave, especially when the *f*-number of the receiver (focal length divided by the diameter of the aperture of the receiver) is large [24]. Fourthly, in uniform media such as water, if no waves propagate in the direction of the receiver, the wave fields cannot be mapped. Even if some waves can reach the receiver, the mapped wave fields will be dependent on the position of the receiver and thus may be inaccurate.

To increase the spatial resolution and avoid the errors caused by a nonuniform scattering coefficient of objects such as biological soft tissues and the position-dependent errors of the receiver when mapping the ultrasound wave fields remotely, the point-spread function (PSF) modulation super-resolution imaging method can be used [25]-[27]. In this method, two measurements of the waves with and without a small modulator introduced at a spatial point can be made (the modulator can be a wave absorber, a scatterer, and/or a phase shifter). Then, one measurement is subtracted from another to obtain a difference caused by the modulator to obtain a super-resolution mapping of the wave fields at that spatial point [25]. Scanning the receiver along with the modulator from one spatial position to another, the entire wave fields in space can be mapped at a spatial resolution determined by the size of the modulator. As the size of the modulator is reduced, the spatial resolution will increase. In theory, there is no limit on the spatial resolution, however in practice, the image resolution is limited by the signal-to-noise ratio (SNR) of the measurement system. Since the modulators can be small and of a uniform size and a uniform property in terms of absorption, scattering, and phase-shift, they can be injected into some objects such as biological soft tissues where there may be channels or a network of blood vessels, to allow an accurate mapping of ultrasound wave fields remotely inside the objects. If the modulator positions inside the objects can be accurately determined by a plane-wave pulse-echo imaging method or other particle localization methods, there will be no distortions to the shape of the mapped ultrasound wave fields. Using multiple modulators can speed up the wave field mapping process if the images of the modulators can be treated individually [25].

In this paper, the PSF-modulation super-resolution imaging method [25]-[26] was used to experimentally map pulse ultrasound wave fields remotely (Fig. 1) at a spatial resolution that is higher than the diffraction-limited resolution of a

receiver (super-resolution) [27] to demonstrate the efficacy of the method. The modulator used was a small spherical glass bead, and the pulse ultrasound wave fields were produced by a focused transducer and a Bessel transducer [28].

The paper is organized as follows. The theory of the PSF-modulation super-resolution imaging method for mapping wave fields is presented in Section II. The experiment method to map pulse ultrasound wave fields and the results are given in Sections III and IV respectively. Finally, a discussion and conclusion are in Section V and VI respectively.

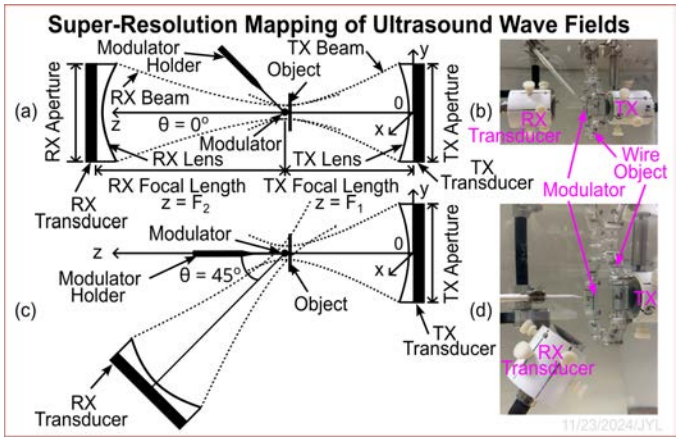

Fig. 1. Setups for mapping pulse ultrasound wave fields (the transmitter was scanned along the x axis) experimentally in water (speed of sound c = 1500 m/s) across the center of the focus of an ultrasound transmitter (the TX transducer with 25.4-mm diameter aperture, 2.25-MHz center frequency, about 61% -6dB relative pulse-echo bandwidth, and an f-number of 1.3) using the PSF-modulation super-resolution imaging method [25]-[27]. The modulator (see Fig. 2(a)) was a small glass bead (0.7-mm diameter) attached to a holder and was fixed with and placed at the focal point of the receiver (the RX transducer that has the same parameters as the transmitter, except that f-number = 1.93). An object can be placed at the focal point of the transmitter. In addition to the wire object in Fig. 2(b), other objects such as biological soft tissues can be used. The setups were also used to map a pulse Bessel beam using the super-resolution method, where the focused transmitter was replaced with a Bessel transducer [28] that was placed about 0.5 mm from the modulator. (a) An experiment setup where the axial axis of the receiver (the RX transducer on the left) was in parallel with that of the transmitter (the TX transducer on the right), i.e., $\theta = 0^{\circ}$. (b) A photo of the setup corresponding to (a) in a water tank. (c) and (d) are the same as (a) and (b) respectively, except that the receiver was rotated by $\theta = 45^{\circ}$ from the axial axis of the transmitter while the modulator was in parallel.

II. Theoretical Preliminaries

Assuming that $f(\vec{r};t)$ represents a spatial wave field (a distribution of the wave in space $\vec{r}$ in a media, for example, the acoustical waves produced by light or electromagnetic heating in photoacoustic imaging [29], waves transmitted through objects such as biological soft tissue, the waves used to illuminate and then scattered or reflected from the object, and waves produced in a uniform media such as water, see the ultrasound waves produced by the TX transducer in Fig. 1) of a wave source at any given time t, an image of the spatial wave field can be reconstructed in a "one-way" process (as opposed to a "two-way" process in pulse-echo ultrasound imaging) [25]:

$$\begin{aligned} R^R(\vec{r};t) &= \int_{t'}\int_{\vec{r}'} \Phi^R(\vec{r}-\vec{r}';t-t')\, f(\vec{r}';t')\, d\vec{r}'\, dt' \\ &= \Phi^R(\vec{r};t) *_{\vec{r},t} f(\vec{r};t) \end{aligned}, \quad (1)$$

where $\Phi^R(\vec{r};t)$ is a spatial-temporal response of a wave receiver (see the RX transducer in Fig. 1), $\vec{r}'$ is an integration variable over the space, t' is an integration variable over the time, $*_{\vec{r},t}$ represents a convolution with respect to both $\vec{r}$ and t, and the superscript "R" represents "receive". Here we assume that the imaging system is a linear shift-invariant (LSI) and linear time-invariant (LTI) system (notice that many practical imaging systems in various areas of science and engineering such as ultrasound and optics can be described or approximately described by an LSI and LTI system and thus it can be represented with the convolution in Eq. (1)).

If $f(\vec{r};t)$ is a point spatial wave field of an infinitely short time duration, i.e., $f(\vec{r};t) = \delta(\vec{r};t)$, where $\delta(\vec{r};t)$ is the Dirac-Delta function [30], from Eq. (1), one obtains the PSF of the imaging system:

$$\begin{aligned} \mathrm{PSF}^R(\vec{r};t) &= \int_{t'}\int_{\vec{r}'} \Phi^R(\vec{r}-\vec{r}';t-t')\,\delta(\vec{r}';t')\, d\vec{r}'\, dt' \\ &= \Phi^R(\vec{r};t) \end{aligned}. \quad (2)$$

Using Eq. (2), Eq. (1) can be written as:

$$R^R(\vec{r};t) = \mathrm{PSF}^R(\vec{r};t) *_{\vec{r},t} f(\vec{r};t). \quad (3)$$

Taking a spatial Fourier transform on both sides of Eq. (3) in terms of $\vec{r}$, one obtains:

$$\begin{aligned} \tilde{R}^R(\vec{k};t) &= \int_{t'} \widetilde{\mathrm{PSF}}^R(\vec{k};t-t')\, \tilde{f}(\vec{k};t')\, dt' \\ &= \widetilde{\mathrm{PSF}}^R(\vec{k};t) *_t \tilde{f}(\vec{k};t) \end{aligned}, \quad (4)$$

where $\tilde{R}^R(\vec{k};t)$, $\widetilde{\mathrm{PSF}}^R(\vec{k};t)$, and $\tilde{f}(\vec{k};t)$ are the spatial Fourier transform of $R^R(\vec{r};t)$, $\mathrm{PSF}^R(\vec{r};t)$, and $f(\vec{r};t)$, respectively, $\vec{k} = (k_x, k_y, k_z)$ is a vector wave number, and $*_t$ represents a convolution with respect to t. From Eq. (4), it is clear that the maximum spatial frequency of the image $R^R(\vec{r};t)$ is limited by that of $\mathrm{PSF}^R(\vec{r};t)$ due to wave diffraction or other limitations such as a large pitch size of a camera sensor or transducer array. The limited maximum spatial frequency of the PSF due to wave diffraction is a fundamental limit to the spatial resolution of an imaging system to image the wave field $f(\vec{r};t)$.

To increase the spatial bandwidth of the imaging system, the PSF function can be multiplied by a complex modulation function $m(\vec{r})$ (the physical meaning of $m(\vec{r})$ is to introduce

a disturbance to an existing PSF of the imaging system by amplitude, phase, or both). The resulting image is given by:

$$R^{R_m}(\vec{r};t) = [\mathrm{PSF}^R(\vec{r};t)m(\vec{r})] *_{\vec{r},t} f(\vec{r};t) + C^R(\vec{r};t), \quad (5)$$

where the subscript "m" of superscript "R" means "modulation" and

$$\begin{aligned} C^R(\vec{r};t) &= \int_{t'}\int_{\vec{r}'} [\mathrm{PSF}^R(\vec{r}';t')\gamma_m^R(\vec{r}')] f(\vec{r}-\vec{r}';t-t')d\vec{r}'dt' \\ &= [\mathrm{PSF}^R(\vec{r};t)\gamma_m^R(\vec{r})] *_{\vec{r},t} f(\vec{r};t) \end{aligned}, \quad (6)$$

where $\gamma_m^R(\vec{r})$ represents the scattering or reflection coefficient of the modulator $m(\vec{r})$. From Eqs. (5) and (6), it is clear that $\gamma_m^R(\vec{r})$ can be viewed as a part of the modulator. Taking a spatial Fourier transform on both sides of Eq. (5), we have:

$$\tilde{R}^{R_m}(\vec{k};t) = [\widetilde{\mathrm{PSF}}^R(\vec{k};t) *_{\vec{k}} \tilde{m}(\vec{k})] *_t \tilde{f}(\vec{k};t) + \tilde{C}^R(\vec{k};t), \quad (7)$$

where $\tilde{R}^{R_m}(\vec{k};t)$, $\widetilde{\mathrm{PSF}}^R(\vec{k};t)$, $\tilde{m}(\vec{k})$, $\tilde{f}(\vec{k};t)$, and $\tilde{C}^R(\vec{k};t)$ are the spatial Fourier transform of $R^{R_m}(\vec{r};t)$, $\mathrm{PSF}^R(\vec{r};t)$, $m(\vec{r})$, $f(\vec{r};t)$, and $C^R(\vec{r};t)$, respectively, and $*_{\vec{k}}$ represents a convolution with respect to $\vec{k}$. Because the convolution with respect to $\vec{k}$ in Eq. (7) is performed in the spatial frequency domain, the maximum spatial frequency of the modulated PSF in Eq. (5), $\mathrm{PSF}^{R_m}(\vec{r};t) = \mathrm{PSF}^R(\vec{r};t)m(\vec{r})$, of the imaging system is increased, making it feasible to reconstruct super-resolution images with methods that are suitable for specific applications in different areas of science and engineering.

In this paper, Eqs. (3) and (5) will be used to reconstruct super-resolution images of broadband pulse ultrasound wave fields.

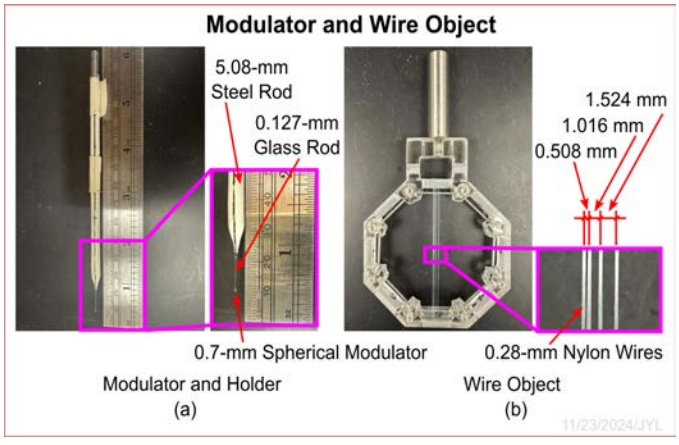

Fig. 2. Photos of (a) a glass bead and (b) a wire object. The glass bead had a diameter of 0.7 mm. It was attached to one end of a glass rod of about 0.127 mm in diameter and about 10 mm in length. The other end of the glass rod was glued to the tip of a tapered steel bar that had a diameter of about 5.08 mm (the steel bar was coated with white epoxy to be water resistant). The wire object contained 4 nylon wires of about 0.28 mm in diameter. The distances between the four wires were about 0.508 mm, 1.016 mm, and 1.524 mm, respectively, as shown in the figure. This wire object was used to introduce high spatial frequency components in the ultrasound wave field to be mapped.

III. Methods

A. Pulse Wave Field of a Focused Transducer

To apply the super-resolution theory in the last section to map a focused pulse ultrasound wave field remotely in water, experiments were conducted (see Fig. 1). In the experiments, the pulse wave field was produced by a 25.4-mm diameter, 2.25-MHz center frequency, and broadband (about 61% -6dB relative pulse-echo bandwidth) PZT transducer (V304, Panametrics, MA, USA). The transducer was electrically driven by a 1-cycle 2.25-MHz sine signal and was focused with a home-made plexiglass lens at about 33.5 mm (*f*-number of about 1.32). The speed of sound of the water was about 1500 m/s and thus the wavelength of the ultrasound pulse at the center frequency was about 0.67 mm. Using the formula given in Eq, (23) of Ref. [25], the one-way full-width-at-half-maximum (FWHM) resolution or beam width of the transmitter is given by:

$$PR_{\mathrm{FWHM}} = 1.41\lambda F_1 / D = 1.24 \text{ mm}, \quad (8)$$

where "R_{FWHM}" represents one-way FWHM resolution of a planar aperture weighting (prefix "P"), $\lambda = c/f$ is the wavelength, c is the speed of sound, f is the center frequency, F_1 is the focal length of the transmitter, and D is the diameter of the transducer.

To map the pulse ultrasound wave field remotely, another PZT transducer that has the same parameters but of a different focal length F_2 of about 49 mm (*f*-number of about 1.93) was used as a receiver. The one-way FWHM diffraction-limited resolution of the receiver is given by:

$$PR_{\mathrm{FWHM}} = 1.41\lambda F_2 / D = 1.81 \text{ mm}, \quad (9)$$

It is clear that the spatial resolution of the receiver is poor when mapping the wave field that only has a FWHM beam width of about 1.24 mm at the focal distance F_1 of the transmitter.

Notice that the beam width of the receiver in Eq. (9) can be used to determine the spatial resolution of an LSI imaging system in Eq. (3). From Eq. (2), it is clear that the spatial-temporal response of the receiver, $\Phi^R(\vec{r};t)$, is the PSF of the LSI imaging system. Assuming that $f(\vec{r};t)$ in Eq. (3) is a geometrical point in space (a spatial Delta function), the image $R^R(\vec{r};t)$ of the point will be the PSF itself. If $f(\vec{r};t)$ consists of two geometrical points that are placed closely with each other, the two points would be indistinguishable in their image unless the distance between the two points is greater than the beam width (the PSF width) given in Eq. (9), which

is a diffraction-limited resolution of the receiver or the imaging system. Using the diffraction-limited PSF to map the wave field with Eq. (3), one can establish a baseline to determine if a method that uses the same receiver to map the same wave field has overcome the diffraction limit (i.e., achieving super-resolution). If the beam width of the mapped wave field is smaller than the baseline beam width that is at least the PSF width in Eq. (9) due to the convolution in Eq. (3), the method breaks the diffraction limit and thus has achieved a super-resolution.

To increase the spatial resolution beyond the diffraction limit of the receiver when mapping the pulse ultrasound wave field, the PSF-modulation super-resolution imaging method [25] was used. To implement the method experimentally, a small glass bead (see Fig. 2(a)) of a diameter of about 0.7 mm was attached to one end of a glass rod of about 0.127 mm in diameter and about 10 mm in length, and the other end of the glass rod was glued to the tip of a tapered steel bar of about 5.08 mm in diameter (Fig. 2(a)). The glass bead was then fixed and placed at the focal point of the receiver for a super-resolution mapping of the ultrasound pulse wave field in the following steps. Assuming that the modulator causes an amplitude modulation by completely blocking the incident ultrasound wave field in the space that the modulator occupies, the modulator can be described as follows (see Fig. 1):

$$m(\vec{r}) = \begin{cases} 0, & |\vec{r} - \vec{r}_{F_1}| \le a \\ 1, & \text{Otherwise} \end{cases}, \tag{10}$$

where $\vec{r}_{F_1} = (x, 0, F_1)$, F_1 is the focal distance of the transmitter (see Fig. 1), and a is the radius of the modulator. Inserting Eq. (10) into Eq. (5), and then subtracting the result from Eq. (3), a super-resolution mapping of the pulse ultrasound wave field can be obtained if the diameter of the modulator is smaller than the diffraction-limited resolution of the receiver given in Eq. (9):

$$\begin{aligned} R^{R_{sub}}(\vec{r};t) &= R^{R}(\vec{r};t) - R^{R_m}(\vec{r};t) \\ &= \mathrm{PSF}^{R_{sub}}(\vec{r};t) *_{\vec{r},t} f(\vec{r};t) - C^{R}(\vec{r};t) \end{aligned}, \tag{11}$$

where

$$\begin{aligned} \mathrm{PSF}^{R_{sub}}(\vec{r};t) &= \mathrm{PSF}^{R}(\vec{r};t)[1 - m(\vec{r})] \\ &= \begin{cases} \mathrm{PSF}^{R}(\vec{r};t), & |\vec{r} - \vec{r}_{F_1}| \le a \\ 0, & \text{Otherwise} \end{cases} \end{aligned} \tag{12}$$

and where the subscript "sub" on the superscript "R" means "subtracted", and $C^{R}(\vec{r};t)$ is due to the scattering or reflections from the modulator $m(\vec{r})$ and is given by Eq. (6) above. From Eq. (12), it is clear that as $a \to 0$, the resulting point-spread function $\mathrm{PSF}^{R_{sub}}(\vec{r};t)$ will behave like a spatial Delta function [30]. In this case, according to Eq. (11), the wave field, $f(\vec{r};t)$, can be reconstructed at an infinitely high spatial resolution. Notice that for an infinitely small modulator ($a \to 0$), the wave scattered from the modulator will be 0 (i.e., $C^{R}(\vec{r};t) \to 0$ in Eq. (6)). If $a > 0$, as was the case in the experiments, the spatial resolution of the mapping of the wave field $f(\vec{r};t)$ will be determined by the diameter of the modulator, and the wave scattered from the modulator $C^{R}(\vec{r};t)$ will not be zero. However, for a given modulator and receiver, the term $\mathrm{PSF}^{R}(\vec{r};t)\gamma_m^{R}(\vec{r})$ in Eq. (6) is fixed, which means that $C^{R}(\vec{r};t)$ depends only on $f(\vec{r};t)$.

To implement Eq. (11) experimentally, a block diagram in Fig. 3 was used. A pulse ultrasound wave field was produced in water by the focused transmitter (TX transducer on the right hand side of the water tank with a focal length of F_1) of the parameters given above. The wave field at the focal distance of the transmitter was received by a focused receiver with a focal length of F_2 (the receiver or the RX transducer on the left hand side of the water tank). To map the wave field at the focal distance of the transmitter, the transmitter was moved (scanned) along the *x* axis in multiple equal-distance steps with a step size of 0.125 mm across the center of transmitter focus (notice that the TX transducer is axially symmetric and thus scanning along the x axis is enough to map the wave filed; also, the motion between the transmitter and receiver is relative and thus one could scan the receiver instead of the transmitter). At each step, an unsynchronized trigger signal was produced from the motor unit and sent to the digitizer unit that produced another trigger signal synchronized to the clock of the digitizer. The synchronized trigger was used to trigger the pulse generator (function generator, HP8116A, Hewlett-Packard Company, CA, USA) to produce a 1-cycle 2.25-MHz electrical sine signal that was amplified by a power amplifier (ENI2100L, Electronics and Innovation, Ltd., NY, USA) to drive the transmitter to produce an ultrasound signal. The ultrasound signal was received to produce an electrical signal that was amplified, filtered by a 0.5-7.5 MHz band-pass filter, digitized at 50 MS/s sampling rate and 12-bit resolution for 512 samples, and then stored on a hard disk. To obtain a super-resolution mapping of the pulse ultrasound wave field at the focal distance of the transmitter, the 0.7-mm diameter modulator mentioned above was placed at the focal point of the receiver. The mapped wave field with the modulator was then subtracted from that without the modulator using Eq. (11) for a super-resolution mapping of the wave field. Notice that the receiver can be placed at different angles as shown in Fig. 1.

To show the versatility of the method for a super-resolution mapping of the pulse ultrasound wave field, an object (see Fig. 2(b)) consisting of 4 nylon wires of diameter of about 0.28 mm with wire spacing of 0.508 mm, 1.016 mm, and 1.524 mm, respectively, was placed at the focus of the transmitter to disturb the wave field to produce higher spatial frequency components in the wave field (notice that in addition to object in Fig. 2(b), other objects such as biological soft tissues can be used). Super-resolution mapping of the wave field with the wire object can be obtained using the

same method as that without the object. In the experiment, the second of the four wires from the left in the wire object (see Fig. 2(b)) was aligned with the center of the transmit focus.

If the object is a biological soft tissue, multiple small modulators can be injected into the tissue through existing channels or a network of blood vessels for super-resolution mapping of the wave field inside the tissue. With multiple small modulators, the speed for the super-resolution wave field mapping can be increase if the diffraction-limited image of each modulator can be isolated, i.e., the modulators are sparse and thus each modulator can be treated individually [25] (the images of the modulators can be obtained by an array transducer to perform a plane-wave pulse-echo imaging [31] or by other particle localization methods). As mentioned in the Introduction, the ability of remotely mapping ultrasound wave fields inside biological soft tissues will be helpful in planning and monitoring of HIFU treatments of tumors (for example, in hyperthermia [32] and histotripsy [33]).

B. Pulse Wave Field of a Bessel Transducer

The method for super-resolution mapping of the focused pulse ultrasound wave field above can be extended to map a pulse Bessel beam [28]. In the experiment, the focused transmitter in Fig. 1 was replaced with a custom 10-ring, 50-mm diameter, 2.5-MHz center frequency, and 1-3 ceramic/polymer composite broadband (about 72% -6dB relative one-way bandwidth) Bessel transducer that had a scaling parameter $\alpha = 1202.45\ \mathrm{m}^{-1}$ of the Bessel function $J_0(\alpha r)$, where r is the radial distance from the transducer axis [28]. The Bessel transducer was electrically driven by a 1-cycle 2.5-MHz sine signal. The 2.25-MHz receiver (RX transducer) and the modulator in Fig. 1 were not changed. The pulse Bessel beam was mapped at 0.5 mm away from the surface of the transducer.

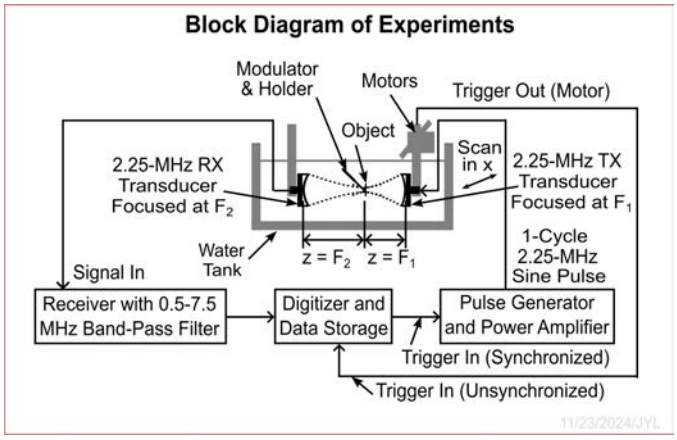

Fig. 3. Black diagram of the experiments. A focused transmitter (TX transducer on the right hand side of the water tank with a focal length of F_1) produced a pulse ultrasound wave field in water. The wave field at the focal distance of the transmitter was received by a focused receiver with a focal length of F_2 (the receiver or the RX transducer on the left hand side of the water tank). To map the wave field at the focal distance of the transmitter, the transmitter was moved (scanned) along the x axis in multiple equal-distance steps across the center of transmitter focus. At each step, an unsynchronized trigger signal was produced from the motor unit and sent to the digitizer unit that produced another trigger signal synchronized to the clock of the digitizer. The synchronized trigger was used to trigger the pulse generator to produce a 1-cycle electrical sine signal that was amplified to drive the transmitter to produce an ultrasound signal. The ultrasound signal was received to produce an electrical signal that was amplified, filtered, digitized, and then stored on a hard disk. To obtain a super-resolution mapping of the pulse ultrasound wave field at the focal distance of the transmitter, a modulator consisting of a small glass bead was placed at the focal point of the receiver. To show the versatility of the method for a super-resolution mapping of pulse ultrasound wave field, a wire object was placed at the focus of the transmitter to disturb the wave field (in addition to the wire object in Fig. 2(b), other objects such as a biological soft tissue can be used).

IV. Results

Figs. 4(a) (see Eq. (3)) and 4(b) (see Eq. (5)) are the pulse ultrasound wave fields mapped experimentally without and with the modulator respectively using the setup in Fig. 1(a), where the axial axis of the RX transducer was in parallel with that of the TX transducer ($\theta = 0^o$) and the object was removed. Subtracting the radio-frequency (RF) signals of the image in Fig. 4(b) from that in Fig. 4(a) resulted in a super-resolution mapping of the wave field in Fig. 4(c) (see Eq. (11)).

To show the flexibility of the super-resolution wave field mapping method, the RX transducer was rotated by an arbitrary angle, say, $\theta = 45^o$ as shown in Figs. 1(c) and 1(d). The results are shown in Figs. 4(d), 4(e), and 4(f) that are corresponding to Figs. 4(a), 4(b), and 4(c), respectively. Fig. 4(d) contains mainly noise since without a modulator, little ultrasound wave can reach the RX transducer at such a large angle (i.e., $R^R(\vec{r};t)$ in Eq. (3) is almost 0) due to the directivity of the focused wave. With a modulator, the scattered wave can be received by the RX transducer and the wave field can be mapped (see Fig. 4(e) that can be described by $R^{R_m}(\vec{r};t)$ of Eq. (5)). This is similar to those studied previously [15]-[23] where a small scatterer (such as the tip of an optical fiber) was used to map ultrasound wave fields at a larger receiver angle close to $\theta = 90^o$. Although the methods in those studies can map ultrasound wave fields at a high spatial resolution, as mentioned before, they do not work if there are other scattering objects such as biological soft tissues near the scatterer, or, if part of the transmit wave can reach the receiver directly as in Fig. 1(a).

The horizontal and vertical dimensions of the images in Fig. 4 represent the time duration (10.24 μs) and the spatial distance (25 mm) along the x axis respectively. The images in Fig. 4 are analytic envelopes of the RF pulse signals and were normalized to their respective maxima.

The FWHM beam widths of the super-resolution pulse ultrasound wave fields in Figs. 4(c) and 4(f) mapped at the focal distance of the transmitter were about 1.13 mm and 1.22 mm respectively, which were close to 1.24 mm calculated from the theory in Eq. (8). The small differences of these beam widths from the theory may be due to an error of the estimated focal distance (33.5 mm) of the transmitter and the fact that for a small spherical object, waves scatter stronger at higher temporal frequencies than those at lower frequencies [34]. The small difference between the beam widths of Figs. 4(c) and 4(f) may be caused by the asymmetry of the modulator (the glass bead was attached to a glass rod) and a

misalignment of the modulator relative to the focal distance of both the RX and TX transducers. Without using the super-resolution wave field mapping method (see Fig. 4(a)), the beam width was much larger (about 2.06 mm) than the theoretical value (1.24 mm), which was due to the large diffraction-limited beam width of the receiver (1.81 mm from Eq. (9)).

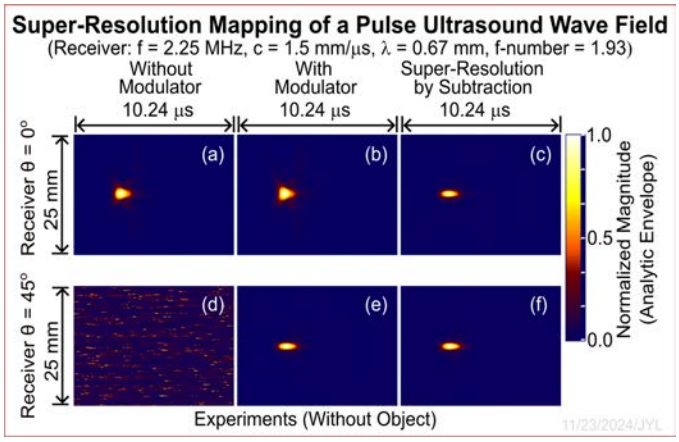

Fig. 4. Super-resolution mapping of a pulse ultrasound wave field without an object (Fig. 1(a)). (a) A focused pulse ultrasound wave field mapped experimentally in water without a modulator using a broadband focused PZT transducer (the RX transducer in Fig. 1). The pulse ultrasound wave field was produced by another PZT transducer (the TX transducer in Fig. 1) that was electrically driven by a 1-cycle sine signal. The pulse wave field at the transmit focal distance was mapped by scanning the TX transducer along the x axis for 25 mm and the signals received were digitized for 10.24 μs. The analytic envelope of the pulse wave field was obtained and normalized to its maximum. The color bar on the righ indicates nomarlized magnitude. (b) is the same as (a) except that the modulator was added (see in Fig. 1(a)). (c) Resulting super-resolution mapping of the pulse ultrasound wave field by subtracting (b) from (a). (d), (e), and (f) are the same as (a), (b), and (c) respectively, except that the RX transducer and the modulator were rotated $\theta = 45^{\circ}$ from the axial axis of the TX transducer (see Fig. 1(c)). Notice that (d) contains mainly noise because of the directivity of the transmit wave.

From Section II "Theoretical Preliminaries", it is clear that the super-resolution wave field mapping method [25]-[27] is applicable to any LSI and LTI systems where the convolution in Eq. (1) is valid, as was illustrated by many examples in Ref. [25]. To show the flexibility of the super-resolution wave field mapping method, the wire object in Fig. 2(b) was placed at the focal distance of the TX transducer (see Fig. 1) to disturb the pulse ultrasound wave field $f(\vec{r};t)$ in Eq. (1). The third wire from the left of the wire object was approximately aligned with the focal point of the TX transducer. The wire object was fixed and scanned with the TX transducer to map the pulse ultrasound wave field. The results are shown in Fig. 5 that is the same as Fig. 4, except that the wire object was added. Compared to Fig. 4, it is seen that high spatial frequency components were produced in the pulse wave field due to the wire object (see Figs. 5(c) and 5(f)). These high spatial frequency components were not seen in Fig. 5(a) where the modulator was not used and the high spatial frequency components were filtered out due to spatial averaging by the receiver that has a poor diffraction-limited resolution (1.81 mm in Eq. (9)).

Notice that in addition to the object in Fig. 2(b), other objects such as biological soft tissues can be placed in the wave field. In this case, the wave field inside the object can be mapped accurately at a high spatial resolution using one or more small modulators [25] if the weak scattering condition of the object is assumed, i.e., multiple scattering, reflection, refraction, and attenuation of the objects can be ignored or compensated (i.e., the LSI and LTI condition is satisfied). Since the modulators can be small, they can be introduced noninvasively into some objects such as biological soft tissues through existing channels or blood vessel network, which may be difficult to do with conventional wave field mapping methods where a small hydrophone, sensor, or optical fiber is used. The flexibility of the super-resolution wave field mapping method can help to map the HIFU beams inside the tissues for tumor targeting and treatment monitoring [32]-[33] at a higher spatial resolution if the positions of the modulators inside the objects can be determined through plane-wave pulse-echo imaging [31] or other particle localization methods.

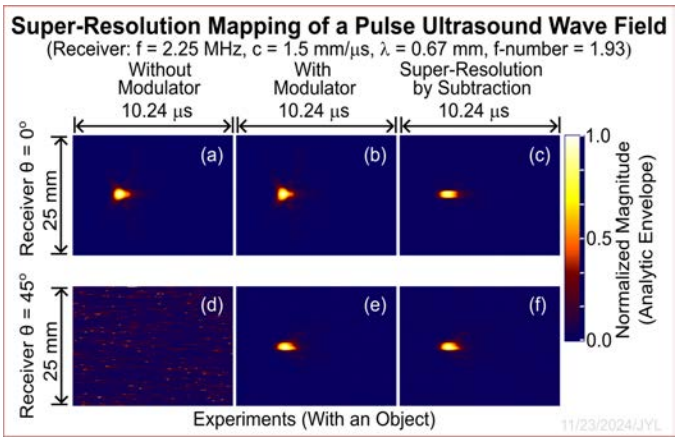

Fig. 5. This figure is the same as Fig. 4 except that a wire object in Fig. 2(b) was placed at the focal distance of the TX transducer (see Fig. 1). The third wire from the left of the wire object was approximately aligned with the focal point of the TX transducer. The wire object was fixed and scanned with the TX transducer to map the pulse ultrasound wave field. Compared to Fig. 4, it is seen that high spatial frequency components were produced in the pulse wave field due to the wire object (see (c) and (f)).

Another example is to experimentally map a pulse Bessel beam [28] using the super-resolution wave field mapping method. In the experiment, a pulse Bessel beam was produced by a 10-ring, 50-mm diameter, 2.5-MHz center frequency, and broadband Bessel transducer [28] that was driven electrically by a 1-cycle sine signal. The pulse Bessel beam was mapped at about 0.5 mm away from the surface of the transducer (notice that the center wavelength of the pulse Bessel beam in water was about 0.6 mm). The TX transducer and the object in Fig. 1 were replaced with the Bessel transducer that was placed near the focal distance of the RX transducer. The results are in Fig. 6 that is the same as Fig. 4 except that the Bessel transducer was used and the dimension along the x axis was 50 mm. From Figs. 6(c) and 6(f) (super-resolution), the high spatial frequency components of the pulse Bessel

beam near the surface of the Bessel transducer can be clearly seen. In comparison, Figs. 6(a) and 6(d) where no modulator was used do not have these high spatial frequency components. Fig. 6(d) shows a part of the incident waves received by the RX transducer at $\theta = 45^{o}$ (see Fig. 1(c)).

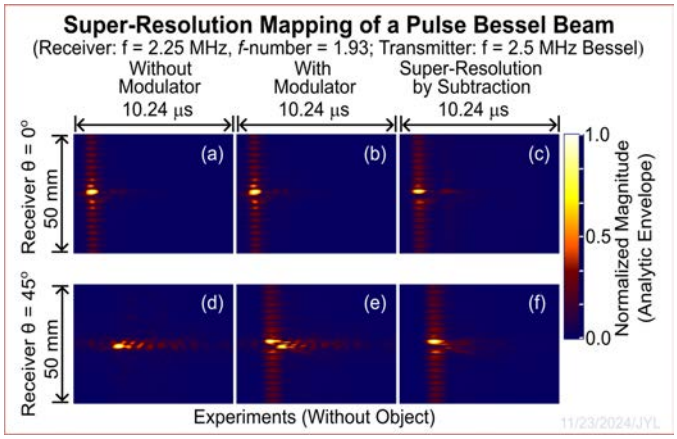

Fig. 6. This figure is the same as Fig. 4 except that a Bessel transducer [28] was used to replace the TX transducer in Fig. 1 and the scanning distance along the x axis was 50 mm. The Bessel transducer had a center frequency of 2.5 MHz and the pulse Bessel beam was produced by a 1-cycle 2.5-MHz electrical sine signal. The Bessel transducer was placed at about 0.5-mm away from the focal distance of the RX transducer that was the same 2.25-MHz transducer used in Fig. 4.

Fig. 7 shows a line plot of the Bessel pulses in Fig. 6 across the center of the Bessel transducer along the x axis (see Fig. 1). The vertical and the horizontal axes of Fig. 7 are the normalized maxima and the lateral distance (along x axis) respectively. The maxima were obtained by finding the maximum value along each row over 400 rows of a panel in Fig. 6. These maxima represent the maximum sidelobes of the mapped pulse Bessel beams. The dotted (pink), solid (black), and dash-dotted (blue) lines in Fig. 7 were obtained from Figs. 6(a), 6(c), and 6(f), respectively. It is clear from Fig. 7 that Figs. 6(c) and 6(f) contain high spatial frequency components and Fig. 6(a) is lack of such components. Thus, the super-resolution wave field mapping method is effective in revealing spatial details of a wave field.

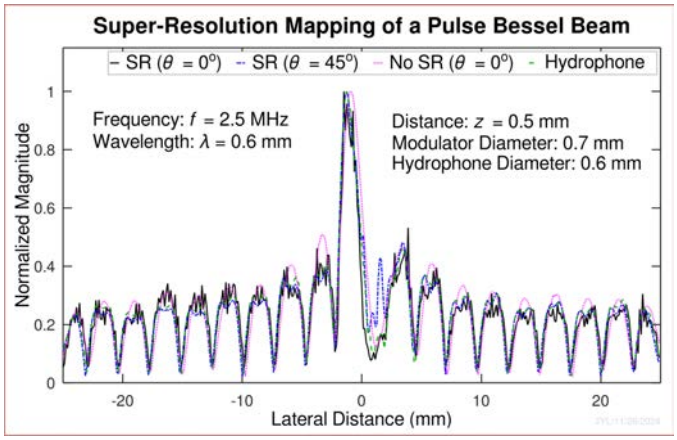

Fig. 7. Line plots of the pulse Bessel beams mapped across the center of the Bessel transducer along the x axis (lateral distance). The solid (black), dash-dotted (blue), dotted (pink), and dashed (green) lines correspond to Figs. 6(c) (super-resolution with RX transducer at $\theta = 0^{o}$), 6(f) (super-resolution with RX transducer at $\theta = 45^{o}$), 6(a) (without super-resolution), and 8(f) (mapped with a PVDF needle hydrophone), respectively. The vertical and horizontal axes represent the normalized magnitude of the pulse Bessel beams and the lateral distance along the x axis respectively. The line plots were normalized to their respective maxima, and they were obtained by taking the maximum from each row of Figs. 6(c), 6(f), 6(a), and 8(f) respectively, which represents the maximum sidelobes of the beams.

For comparison, a PVDF needle hydrophone of 1-20 MHz bandwidth and 0.6 mm diameter of active element (TNU001A, NTT Systems, Inc., Seattle, Washington, USA) was used to map the pulse ultrasound wave fields experimentally. In the experiments, the RX transducer in Fig. 1(a) was replaced with the hydrophone to map the pulse ultrasound wave field at the focal distance of the TX transducer with (Fig. 8(b)) and without (Fig. 8(a)) the wire object in Fig. 2(b). The hydrophone also was placed at about 0.5 mm away from the surface of the Bessel transducer to map the pulse Bessel beam (see Fig. 8(c)). The resulting focused pulse ultrasound wave fields with and without the wire object is shown in Figs. 8(e) and 8(d) respectively, and the resulting pulse Bessel beam mapped using Fig. 8(c) is given in Fig. 8(f). A line plot of Fig. 8(f) is shown as the green dashed line in Fig. 7. Compare the line plot of Fig. 8(f) with those obtained from Figs. 6(c) and 6(f), it is clear that they all contain the high spatial frequency components, as opposed to that (the smooth pink dotted line) obtained from Fig. 6(a). Compare Figs. 8(d), 8(e), and 8(f) with Figs. 4(c), 5(c), and 6(c) respectively, they are similar except that the pulse lengths in Figs. 8(d), 8(e), and 8(f) are shorter. This is because the hydrophone used has a much wider bandwidth (1-20 MHz) than the RX transducer used in Figs. 4(c), 5(c), and 6(c). The beam width of the pulse wave field in Fig. 8(d) was about 1.41 mm, which is larger than the theoretical value of 1.24 mm due to the size of the active element of the hydrophone.

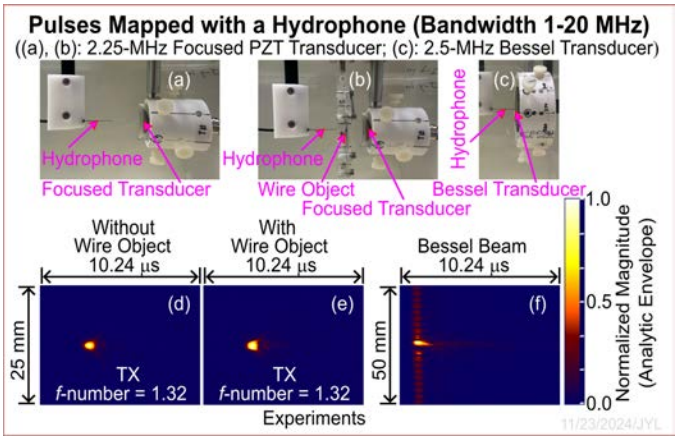

Fig. 8. Focused pulse ultrasound wave fields mapped with a broadband PVDF needle hydrophone at the focal distance of the TX transducer with ((b) and (e)) and without ((a) and (d)) the wire object in Fig. 2(b), and a pulse Bessel beam mapped by the hydrophone at 0.5 mm away from the surface of the Bessel transducer [28] ((c) and (f)). (a), (b), and (c) are photos of the

experiment setups corresponding to (d), (e), and (f) respectively. The wave fields in (d), (e), and (f) are the same as those in Fig. 4(a), 5(a), and 6(a), respectively, except that the hydrophone was used to map the wave fields.

V. Discussion

The results of the super-resolution wave field mapping method show that the method is effective in achieving a high spatial resolution when mapping the wave fields. The method also works whether a part of the transmit wave can reach the receiver or not (see Figs. 4 and 5 with $\theta = 0^o$ and 45^o). In addition, the method works when there is an object placed in the wave field to be mapped (see Fig. 5), which allows the method to map the wave field inside an object such as biological soft tissue under the conditions mentioned previously in Section IV "Results". As the size of the modulator decreases, the spatial resolution of the mapped wave field will increase.

Despite the spatial resolution can be increased by the super-resolution wave field mapping method, the highest spatial resolution that can be achieved is limited by the signal-to-noise ratio of the experiment system, as was discussed in Ref. [25]. Also, the dynamic range of the system will affect the highest achievable spatial resolution [25]. If the received waves come only from those scattered from the modulator, less dynamic range is needed since no subtraction is necessary for super-resolution mapping of the wave fields (see Fig. 1(c) and Figs. 4(d), 4(e), and 4(f)).

The quantitative value of the mapped wave field with the super-resolution method not only depends on the geometry (shape, size, focal length) and the sensitivity of the receiver, but also depends on the size and shape of the modulator. If the size of the modulator becomes much smaller as compared to the minimum wavelength of the wave field, the modulator will be close to a point scatterer, absorber, or phase shifter. In this case, the shape of the modulator will not have much effect. However, as the size of the modulator increases, the effects of the shape and orientation of the modulator may be significant. Thus, to quantitatively map a wave field, the factors of the modulator need to be taken into consideration. However, if the modulator is small and has a fixed shape, size, and material prosperity, its effects on the wave field will be small and constant, and thus can be compensated when mapping the wave field. If the modulator is spherically symmetric, i.e., a sphere, the compensation on the shape and orientation of the modulator is not necessary due to the symmetry even if the size of the modulator is not small compared to the wavelength. This in fact is another advantage of the PSF-modulation super-resolution imaging method to map the wave field over the conventional method that uses a needle hydrophone since it would be very difficult to make a spherically symmetric hydrophone of the size of a needle hydrophone (usually 0.6 mm or smaller) and also take care of all electronic connections and wiring.

In many cases such as HIFU, the ultrasound wave field is highly distorted in terms of time. This means that the wave field to be mapped may have high temporal frequency components (harmonics). In this case, to quantitatively map the wave field, not only the frequency response of the receiver needs to be considered, but also the frequency-dependent property of the modulator needs to be taken into account. When a small modulator is used, it can be viewed as a high-pass filter to the impinging wave since the modulator will scatter waves more strongly at a higher temporal frequency. Thus, a compensation for the frequency dependency of the modulator is needed to obtain a quantitative wave field mapping.

In this paper, a small glass bead was used as a modulator. However, the modulator can be made of any type of material such as metals, plastics, ceramics, wave absorbers, magnetic particles, and so on, depending on applications. The modulation to the wave field can be amplitude, absorption, phase shift, and a combination of them [25], and a choice of the modulation also depends on applications.

As can be seen from Fig. 1, the super-resolution wave field mapping method allows the receiver to be placed remotely from the wave field to be mapped while reducing the spatial averaging effect due to a poor diffraction-limited spatial resolution of the receiver, especially when the receiver has a large *f*-number. Placing the receiver remotely is advantageous when it is not practical to place the receiver directly in the wave field to be mapped. For example, it could be difficult to insert a receiver into an object to map the ultrasound wave field inside the object, while it would be easier to inject small modulators (particles) into some objects such as biological soft tissues where there may be channels or a network of blood vessels. Also, a receiver such as a delicate PVDF hydrophone can be damaged if it is placed in the media or objects within which the environment is corrosive, has a high temperature, or has high wave intensity. In these cases, super-resolution mapping of wave fields can be used by choosing suitable modulators.

VI. Conclusion

A PSF-modulation super-resolution imaging method [25]-[27] was successfully applied to map pulse ultrasound wave fields remotely at a high spatial resolution [27]. The theoretical background of the method was given and experiments were conducted. In the experiments, pulse ultrasound wave fields were produced by a broadband focused PZT transducer and a 1-3 ceramic/polymer composite broadband Bessel transducer [28], driven electrically by a 1-cycle sine signal. The PZT transducer had a 2.25-MHz center frequency, about 61% -6dB relative pulse-echo bandwidth, 25.4-mm diameter, and an *f*-number of about 1.32. The Bessel transducer had a 2.5-MHz center frequency, about 72% -6dB relative one-way bandwidth, 50-mm diameter, and 10 annular rings. Another focused PZT transducer of the same parameters above but with an *f*-number of about 1.93 was used as a receiver to map the pulse ultrasound wave fields remotely. A modulator made of a glass bead of 0.7-mm diameter was used to achieve a super-resolution in mapping the pulse ultrasound wave fields. Different orientations of the receiver ($\theta = 0^o$ and 45^o relative to the axial axes of the transmit transducers) were used in the experiments. A wire object was used to disturb the pulse ultrasound wave fields to be mapped to show versatility of the method. In addition, a broadband (1-20 MHz) PVDF needle hydrophone was used to map the pulse ultrasound

wave fields for comparison. The results show that the super-resolution wave field mapping method can achieve a high spatial resolution when mapping pulse ultrasound wave fields remotely, overcoming the diffraction limit of the receiver and opening up a possibility of mapping wave fields inside some objects such as biological soft tissues.

REFERENCES

[1] S. Hisatake, H. Nakajima, H. H. N. Pham, H. Uchida, M. Tojyo, Y. Oikawa, K. Miyaji, and T. Nagatsuma. "Mapping of electromagnetic waves generated by free-running self-oscillating devices." *Scientific Reports* 7, no. 1 (2017): 9203.

[2] S. Koziel and A. Pietrenko-Dabrowska. "Fast EM-driven nature-inspired optimization of antenna input characteristics using response features and variable-resolution simulation models." *Scientific Reports* 14, no. 1 (2024): 10081.

[3] J. Krupka. "Microwave measurements of electromagnetic properties of materials." *Materials* 14, no. 17 (2021): 5097.

[4] H. Wang, D. Zeng, Z. Chen, and Z. Yang. "A rapid and non-invasive method for measuring the peak positive pressure of HIFU fields by a laser beam." *Scientific Reports* 7, no. 1 (2017): 850.

[5] B. Karaböce, S. Nur, and A. Şahin. "High Intensity Focused Ultrasound Pressure Field Characterization." In *2020 IEEE International Instrumentation and Measurement Technology Conference (I2MTC)*, pp. 1-6. IEEE, 2020.

[6] P. R. Patel, A. Luk, A. Durrani, S. Dromi, J. Cuesta, M. Angstadt, M. R. Dreher, B. J. Wood, and V. Frenkel. "In vitro and in vivo evaluations of increased effective beam width for heat deposition using a split focus high intensity ultrasound (HIFU) transducer." *International journal of hyperthermia* 24, no. 7 (2008): 537-549.

[7] D. A. Hutchins and G. Hayward. "Radiated fields of ultrasonic transducers." In *Physical Acoustics*, vol. 19, pp. 1-80. Academic Press, 1990.

[8] W. Lee and Y. Roh. "Ultrasonic transducers for medical diagnostic imaging." *Biomedical engineering letters* 7, no. 2 (2017): 91-97.

[9] J. W. Hunt, M. Arditi, and F. Stuart Foster. "Ultrasound transducers for pulse-echo medical imaging." *IEEE Transactions on Biomedical Engineering* 8 (1983): 453-481.

[10] J. A. Jensen. "Medical ultrasound imaging." *Progress in biophysics and molecular biology* 93, no. 1-3 (2007): 153-165.

[11] J. D. Achenbach. "Quantitative nondestructive evaluation." *International Journal of Solids and Structures* 37, no. 1-2 (2000): 13-27.

[12] E. Martin and B. Treeby. "Investigation of the repeatability and reproducibility of hydrophone measurements of medical ultrasound fields." *The Journal of the Acoustical Society of America* 145, no. 3 (2019): 1270-1282.

[13] P. C. Beard, A. M. Hurrell, and T. N. Mills. "Characterization of a polymer film optical fiber hydrophone for use in the range 1 to 20 MHz: A comparison with PVDF needle and membrane hydrophones." *IEEE Transactions on ultrasonics, ferroelectrics, and frequency control* 47, no. 1 (2000): 256-264.

[14] X. M. Lu and T. L. Proulx. "Single crystals vs. PZT ceramics for medical ultrasound applications." In *IEEE Ultrasonics Symposium*, vol. 1, pp. 227-230. 2005.

[15] G. Xing, V. Wilkens, and P. Yang. "Review of field characterization techniques for high intensity therapeutic ultrasound." *Metrologia* 58, no. 2 (2021): 022001.

[16] Y. Liu, K. A. Wear, and G. R. Harris. "Uncertainty of High Intensity Therapeutic Ultrasound (HITU) Field Characterization with Hydrophones: Effects of Nonlinearity, Spatial Averaging, and Complex Sensitivity." *Ultrasound in medicine & biology* 43, no. 10 (2017): 2329.

[17] O. A. Sapozhnikov, M. R. Bailey, P. J. Kaczkowski, V. A. Khokhlova, and W. Kreider, "Portable acoustic holography systems for therapeutic ultrasound sources and associated devices and methods." U.S. Patent 9,588,491, issued March 7, 2017.

[18] K. Raum and W. D. O'Brien, "Pulse-echo field distribution measurement technique for high-frequency ultrasound sources." *ieee transactions on ultrasonics, ferroelectrics, and frequency control* 44, no. 4 (1997): 810-815.

[19] P. Kaczkowski, B. Cunitz, V. Khokhlova, and O. Sapozhnikov. "High resolution mapping of nonlinear MHz ultrasonic fields using a scanned scatterer." In *IEEE Symposium on Ultrasonics, 2003*, vol. 1, pp. 982-985. IEEE, 2003.

[20] M. E. Schafer, J. Gessert, and W. Moore. "Development of a High Intensity Focused Ultrasound (HIFU) hydrophone system." In *IEEE International Ultrasonics Symposium*, pp. 1739-1742, 2005.

[21] M. E. Schafer, J. Gessert, and W. Moore, "Development of a high intensity focused ultrasound (HIFU) hydrophone system." In *AIP Conference Proceedings*, vol. 829, no. 1, pp. 609-613. American Institute of Physics, 2006.

[22] M. E. Schafer and J. Gessert. "Development of a high intensity focused ultrasound (HIFU) hydrophone system." In *AIP Conference Proceedings*, vol. 1113, no. 1, pp. 301-305. American Institute of Physics, 2009.

[23] Y. Wang and F. Ye. "The measurement of HIFU field using a reflective needle hydrophone." In *AIP Conference Proceedings*, vol. 911, no. 1, pp. 3-7. American Institute of Physics, 2007.

[24] J. W. Goodman. *Introduction to Fourier optics*. Roberts and Company publishers, 2005.

[25] Jian-yu Lu, "Modulation of Point Spread Function for Super-Resolution Imaging." *IEEE Transactions on Ultrasonics, Ferroelectrics, and Frequency Control* , vol. 71, no. 1, pp. 153-177, January 2024.

[26] Jian-yu Lu, "A general method to obtain clearer images at a higher resolution than theoretical limit," 186th Meeting of Acoustical Society of America, Acoustical Lay Language Paper, April 22, 2024 (https://acoustics.org/a-general-method-to-obtain-clearer-images-at-a-higher-resolution-than-theoretical-limit/).

[27] Jian-yu Lu, "Super-resolution mapping of wave field using a receiver from a far distance," in *2024 IEEE Ultrasonics, Ferroelectrics, and Frequency Control Joint Symposium (UFFC-JS) Proceedings*, pp.1-4, 2024. DOI: https://doi.org/10.1109/UFFC-JS60046.2024.10793602

[28] Jian-yu Lu and J. F. Greenleaf, "Ultrasonic nondiffracting transducer for medical imaging," IEEE Transactions on Ultrasonics, Ferroelectrics, and Frequency Control, vol. 37, no. 5, pp. 438-447, September 1990.

[29] M. Xu and L. V. Wang. "Photoacoustic imaging in biomedicine." *Review of scientific instruments* 77, no. 4 (2006).

[30] S. C. Gupta, "Delta function." *IEEE Transactions on Education* 1 (1964): 16-22.

[31] Jian-yu Lu, "2D and 3D high frame rate imaging with limited diffraction beams," *IEEE Transactions on Ultrasonics, Ferroelectrics, and Frequency Control*, vol. 44, no. 4, pp. 839-856, July 1997

[32] C. J. Diederich and Kullervo Hynynen. "Ultrasound technology for hyperthermia." *Ultrasound in medicine & biology* 25, no. 6 (1999): 871-887.

[33] Z. Xu, T. D. Khokhlova, C. S. Cho, and V. A. Khokhlova. "Histotripsy: a method for mechanical tissue ablation with ultrasound." *Annual Review of Biomedical Engineering* 26 (2024).

[34] N. A. Logan. "Survey of some early studies of the scattering of plane waves by a sphere." *Proceedings of the IEEE* 53, no. 8 (1965): 773-785.

Jian-yu Lu (S'86--M'88--SM'99--F'08--LF'25) received the B.S. degree in physics/electrical engineering from Fudan University, Shanghai, China, in February 1982; the M.S. degree in physics/acoustics from Tongji University, Shanghai, China, in 1985; and the Ph.D. degree in biomedical engineering from Southeast University, Nanjing, China, in 1988. From December 1988 to February 1990, he was a Postdoctoral Research Fellow with the Mayo Medical School, Rochester, Minnesota, USA.

He was an Associate Professor of biophysics with the Mayo Medical School and an Associate Consultant with the Department of Physiology and Biophysics, Mayo Clinic/Foundation, Rochester, Minnesota, USA. Since 1997, he has been a full Professor with the Department of Bioengineering, The University of Toledo (UT), Toledo,

OH, USA, where he also has been an Adjunct Professor with the College of Medicine and Life Sciences, since 1998. His research interests are in acoustic imaging, devices, tissue identification; medical ultrasonic transducers; ultrasonic beam forming; and wave propagation physics.

Dr. Lu received the Outstanding Paper Award from the IEEE UFFC Society (UFFC-S) for two of his papers published in the IEEE Transactions on Ultrasonics, Ferroelectrics, and Frequency Control (TUFFC) in 1992 for the discovery of X wave that, in theory, is both diffraction and dispersion free. Both phase and group velocities of the X wave are faster than the speed of sound (supersonic) or light in vacuum (superluminal) (see newly-developed superluminal X wave in quantum mechanics in 2023 at IEEE TechRxiv https://doi.org/10.36227/techrxiv.22083719.v2 and 2023 IEEE IUS https://doi.org/10.1109/IUS51837.2023.10306675). In addition, he received the Edward C. Kendall Award for his meritorious research from the Mayo Alumni Association in 1992, the NIH FIRST Award in 1991, Distinguished Service Award from UFFC-S in 2016, and the Engineer of the Year Award from the IEEE Toledo Section in 2021.

He served as the President of IEEE UFFC-S from 2014 to 2015, the Editor-in-Chief of IEEE TUFFC from 2002 to 2007, the General Chair of the 2008 IEEE International Ultrasonics Symposium (IUS), the Technical Program Committee (TPC) Chair of 2001 IEEE IUS, a member of the Editorial Board of IEEE Access from 2016 to 2021, an Elected AdCom member of IEEE UFFC-S from 2009 to 2011, and many committees of UFFC-S. In addition, he served in IEEE Toledo Section.

He is a Fellow of IEEE (conferred in 2008), the American Institute of Ultrasound in Medicine (AIUM) (conferred in 2005), and the American Institute for Medical and Biological Engineering (AIMBE) (conferred in 2007).